Modeling of Vinylidene Fluoride Heterogeneous Polymerization in Supercritical Carbon Dioxide

Philipp A. Mueller, Giuseppe Storti, and Massimo Morbidelli*

Swiss Federal Institute of Technology Zurich, ETHZ, Institut für Chemie- und Bioingenieurwissenschaften, ETH−Hönggerberg/HCI, CH-8093 Zurich, Switzerland

Marco Apostolo

Solvay Solexis S.p.A., World Headquarters, Viale Lombardia 20, I-20021 Bollate (MI), Italy

Roland Martin

SOLVIN S.A., Solvay Research & Technology Center, Rue de Ransbeek 310, B-1120 Brussels, Belgium

Received March 3, 2005; Revised Manuscript Received May 23, 2005

ABSTRACT: The heterogeneous polymerization of vinylidene fluoride in supercritical carbon dioxide has been investigated experimentally, and the obtained results have been interpreted through a detailed kinetic model. The comparison between model predictions and experimental data indicates the presence of two reaction loci: the continuous supercritical phase and the dispersed polymer phase. However, the presence of two reaction loci is not the result of the thermodynamic partitioning between two phases, but rather a kinetic effect. This in fact occurs because part of the radicals generated in the continuous phase, which are driven by thermodynamic equilibrium to diffuse to the dispersed phase, are actually terminated in the former before they can reach the latter. This provides a quantitative explanation for the bimodal molecular weight distributions often measured experimentally for this system.

1. Introduction

In our previous contributions,[1,2] a detailed model for dispersion polymerization in supercritical carbon dioxide ($scCO_2$) was developed and applied to the case of methyl methacrylate (MMA) polymerization. The main features of this model with respect to similar models previously reported in the literature are (i) it accounts for two reaction loci, the supercritical continuous phase and the dispersed particles, and (ii) it includes the detailed description of the interphase mass transport of the active polymer chains as a function of their length.

In the case of MMA dispersion polymerization in $scCO_2$, it was found that the amount of polymer chains produced (i.e., terminated) in the continuous phase is negligible compared to that produced in the polymer particles. This is due to the fact that the interphase transport of radical chains from the continuous to the dispersed phase is much faster than the bimolecular termination within the former. Consequently, the radical chains which are predominantly produced in the continuous phase diffuse into the particles before they terminate. These findings were confirmed experimentally, in particular through the measured molecular weight distributions (MWD) which were found to be monomodal and made of chains grown in the dispersed phase.[2]

A different kinetic behavior has been reported in the case of vinylidene fluoride (VDF) polymerization in $scCO_2$, in particular resulting in very broad, bimodal MWDs. Although the presence of two polymerization loci with different reaction rates could be an obvious explanation of these findings,[3] other mechanisms have been considered. In particular, the presence of a chain transfer to polymer reaction[3,4] has been shown to account for the breadth of the MWD but not for its bimodality, while imperfect mixing in the case of continuous polymerization[4] has been found not to significantly affect the MWD.

In this work we intend to investigate this particular aspect and, more in general, to provide a complete description of the kinetics of this system. The detailed kinetic model mentioned above has been extended to the VDF precipitation polymerization in $scCO_2$, and its predictions have been compared with the results of polymerization experiments carried out at different pressure and monomer concentration values. It is worth mentioning that, due to the complexity of the system, the corresponding detailed models include inevitably a very large number of parameters. Thus, to obtain a reliable model, a specific effort has been made to estimate most of the model parameters a priori, i.e., from independent sources, minimizing any direct fitting to the experimental polymerization data.

2. Experimental Section

All experiments have been carried out at Solvay Research & Technology Center in Brussels using a 2 L stainless steel autoclave with maximum operating pressure of 39.5 MPa at 150 °C. The reactor was equipped with a jacket connected to a heating/cooling circulator (−40 to 150 °C), magnetically coupled stirrer with measured and controlled speed accommodating different agitator types, pressure transducer, Pt-100, and Inconel rupture disk connected to a blow-down tank. A 45 °C pitched blade agitator with upward pumping action was used at a rotational speed of 300 rpm. The reactor and

* To whom correspondence should be addressed: e-mail massimo.morbidelli@chem.ethz.ch; phone +41-1-6323034; Fax +41-1-6321082.

10.1021/ma0504522 CCC: $30.25
Published on Web 07/06/2005

Table 1. Operating Conditions and Recipes of the Experimental Runs

run	DEPDC [mol L^{-1}]	VDF [mol L^{-1}]	T [°C]	ρ [kg L^{-1}]	p_0 [MPa]
1	5×10^{-3}	3.1	50	0.79	20.4
2	5×10^{-3}	1.0	50	0.79	20.4
3	5×10^{-3}	6.2	50	0.79	20.4
4	5×10^{-3}	3.1	50	0.65	13.3
5	5×10^{-3}	3.1	50	0.89	33.2

the different lines could be vented, evacuated, and purged with nitrogen. CO_2 and VDF were fed to the reactor in liquid form by means of cooled, plunger-type metering pumps. The supply tanks were placed on precision balances allowing for the control of the quantities (precision of 1 g). Samples were extracted from the reactor into a 25 mL stainless steel high-pressure cylinder by expanding a small amount of reaction mixture through a filter to low pressure so as to stop the polymerization immediately. The unit was equipped with a supervisory control and data acquisition system.

2.1. Materials. VDF was obtained from the Solvay plant Tavaux (F) and used as received. CO_2 grade 4.8 was used as received. Diethyl peroxydicarbonate (DEPDC) was synthesized in a 500 mL three-necked flask equipped with thermometer, dropping funnel, and reflux condenser. The synthesis procedure was the following: 100 mL of demineralized H_2O was cooled to about 5 °C by an ice/water bath. Under stirring, 12 mL of ethyl chloroformate and 6.64 g of a 30% H_2O_2 solution were added to the flask. Next, 24 mL of a 5 N NaOH solution was added slowly via the dropping funnel so that the temperature did not rise above 10 °C. The reaction mixture was allowed to stir for another 10 min at about 5 °C. Afterward, 50 mL of precooled 1,1,1,3,3-pentafluorobutane ($T \approx 5$ °C) was added under increased stirring speed. The organic phase was separated after 5 min in a separation funnel and collected in a graduated Schott glass. The water phase was extracted a second time with 46 mL of precooled solvent. The collected organic phases were mixed and completed to 100 mL at 5 °C (concentration: approximately 10 g/100 mL). The analysis for active oxygen was done by dissolving 100 mg of $FeCl_3$ in 10 mL of water (catalyst solution) and 10 g of KI in 40 g of water (20% solution). 100 mL of acetic acid was mixed with 100 mL of 2-propanol. Under stirring the two solutions were combined under N_2 atmosphere for 30 min. 1 mL of the DEPDC solution was added to 20 mL of the KI solution, and afterward 2 drops of the $FeCl_3$ solution were added. After 15 min stirring at room temperature, the free iodine was titrated with the $Na_2S_2O_3$ solution (0.05 N). The same procedure was used for the blank reagents. Obtained yields in peroxide were typically between 89% and 92%.

2.2. Reaction Procedure. In a typical polymerization reaction, a weighted quantity of the DEPDC initiator solution (100 g L^{-1} in 1,1,1,3,3-pentafluorobutane, synthesized by the procedure described above) was injected by a syringe in the open reactor, cooled to −5 °C. The solvent was then completely evaporated by applying vacuum, followed by five nitrogen purging and vacuum cycles to eliminate all traces of air. The stirrer was turned on, and part of the total amount of CO_2 (80%) was then pumped as liquid to the autoclave, followed by the feeding of the liquid VDF. Next, the reactor was heated under stirring to the reaction temperature (50 °C). Once the temperature was stabilized at the set point, an additional quantity of CO_2 was pumped in to reach the desired pressure. Finally, after a predetermined pressure drop, the autoclave was cooled to 40 °C, and the pressure was isothermally released through a heated control valve. Residual VDF and CO_2 were eliminated by applying vacuum for 3 h.

Experiments at three different initial monomer concentrations as well as three different densities (pressures) were carried out. A summary of operating conditions and recipes is given in Table 1.

2.3. Analytical Techniques. To monitor the time evolution of the reaction, samples were withdrawn from the reactor at different times. The amount of polymer produced was evaluated by gravimetry, and the complete MWD was measured by gel permeation chromatography (GPC). These measurements were performed by preparing solutions of PVDF at 1 g L^{-1} in *N,N*-dimethylformamide (DMF, HPLC quality grade)/0.1 mol L^{-1} LiBr under heating (60 °C) and under stirring for 30 min. A Waters Alliance 2690 separation module equipped with Waters μ-Styragel HR type columns (2 × HR-5E, 1 × HR-2) and a Waters 2410 refractive index detector were used at 40 °C, flow rate of 1 mL min^{-1}, and injected sample volume 100 μL. The molecular weight analysis is based on the universal calibration procedure with PMMA narrow standards. The viscosity−molecular weight relationship for PVDF has been checked by the independent determination of the molecular weight using static light scattering in *N,N′*-dimethyl-*N,N′*-trimethylene urea as the most suitable solvent. The Mark−Houwink constants used are $K = 1.32 \times 10^{-4}$ dL g^{-1}, $a = 0.674$ (PMMA), $K = 5.63 \times 10^{-5}$ dL g^{-1}, and $a = 0.803$ (PVDF).

3. Model Development

As mentioned above, the general model for heterogeneous polymerization in supercritical CO_2 developed and applied to the dispersion polymerization of MMA in previous studies[1,2] has been used. Therefore, only a short description of the model is reported below, with special attention to the few changes requested by the specificity of the VDF precipitation polymerization.

3.1. Model Assumptions, Kinetic Scheme, and Interphase Equilibria. The main characteristics of the model are as follows: (1) Two reaction loci are considered: the polymer-rich dispersed phase and the CO_2-rich continuous phase. (2) Low molecular weight species (solvent, initiator, and monomer) undergo very fast transport between the phases and are therefore assumed to be at equilibrium conditions at all times. For larger molecular weight species the model describes the kinetics of the interphase mass transport. (3) A chain length dependent partition coefficient for polymer chains between continuous and dispersed phase is considered. (4) The process of particle formation or nucleation is not simulated, and a constant number of particles is assumed throughout the entire process. This is because the nucleation period where the particle number changes significantly is expected to be very short in these systems.[5,6] It is worth noting that no stabilizer is used, and as a consequence, a polymer powder made of irregular fragments of different sizes is typically found experimentally. However, since the model needs to estimate the specific particle surface area, a_p, as a function of conversion, X, the following relation has been used:

$$a_p = \left(\frac{X^f}{X}\right)^{1/3} a_p{}^f \tag{1}$$

where $a_p{}^f$ is the a_p value at $X = X^f$ and is used as an adjustable parameter. As discussed later in detail, this relation is compatible with spherical polymer particles in constant number. (5) The crystalline part of the polymer is assumed to be impermeable to all species and therefore neglected when evaluating interphase partitioning of the various species.

The kinetic scheme considered for VDF polymerization includes, besides the usual initiation and propagation reactions, bimolecular termination both by combi-

nation and by disproportionation as well as chain transfer to polymer:

initiation:
$$I_j \xrightarrow{k_{dj}} 2I_j^{\bullet}$$
$$I_j^{\bullet} + M_j \xrightarrow{k_{1j}} R_{1,j}$$

propagation:
$$R_{x,j} + M_j \xrightarrow{k_{pj}} R_{x+1,j}$$

termination:
$$R_{x,j} + P_{y,j} \xrightarrow{k_{fpj}} P_{x,j} + R_{y,j}$$
$$R_{x,j} + R_{y,j} \xrightarrow{k_{tdj}} P_{x,j} + P_{y,j}$$
$$R_{x,j} + R_{y,j} \xrightarrow{k_{tcj}} P_{x+y,j}$$

Note that, when two subscripts are given, the first one (x or y; $x, y = [1, \infty]$) indicates the chain length and the second one the phase ($j = 1$ for the continuous phase and $j = 2$ for the dispersed phase). The same kinetic scheme, but with different values of the kinetic rate constants, is applied to both phases.

About the description of the interphase equilibrium partitioning of the low molecular weight species, the Sanchez−Lacombe model[7,8] was used for monomer and solvent, while for the initiator a constant partition coefficient was used.[1]

3.2. Equations. The basic model equations are the mass balances of the low molecular weight species (monomer, solvent, and initiator) and of the active and terminated polymer chains, which are reported in the following. The meaning of all variables is detailed in the Notation section. Symbols in square brackets have to be intended as molar concentrations and without brackets as numbers of moles.

Low Molecular Weight Species. The material balances of these species are the same as those reported in ref 1, while the equations describing the interphase partitioning have been changed as follows.

When using the Sanchez−Lacombe equation of state (EOS) to model phase behavior and partitioning of a specific system, three characteristic parameters, ϵ^*, v^* and r, are needed for both pure components and mixtures. While the values of these quantities for the pure components are usually evaluated by fitting independent experimental data of some suitable single-component thermodynamic property (cf. refs 7 and 8), for the mixture appropriate mixing rules are typically used. In this work, the mixing rules proposed by McHugh and Krukonis[9] for a system of nc components have been selected:

$$v^*_{mix} = \sum_{i=1}^{nc}\sum_{j=1}^{nc}\phi_i\phi_j v^*_{ij} \tag{2}$$

with

$$v^*_{ij} = \frac{v^*_{ii} + v^*_{jj}}{2}\eta_{ij} \tag{3}$$

where η_{ij} is an empirical binary parameter accounting for deviations from the arithmetic mean of the parameter v^*_{ij}. The volume fraction ϕ_i is defined as

$$\phi_i = \frac{\omega_i}{\rho^*_i v^*_i}\Big/\sum_{j=1}^{nc}\left(\frac{\omega_j}{\rho^*_j v^*_j}\right) \tag{4}$$

where ω_i is the mass fraction of component i in the mixture, and ρ^*_i and v^*_i are the characteristic mass density and close-packed molar volume of component i, respectively. The mixing rule for the characteristic interaction energy, ϵ^*_{mix} is given by

$$\epsilon^*_{mix} = \frac{1}{v^*_{mix}}\sum_{i=1}^{nc}\sum_{j=1}^{nc}\phi_i\phi_j\epsilon^*_{ij}v^*_{ij} \tag{5}$$

with

$$\epsilon^*_{ij} = (\epsilon^*_{ii} + \epsilon^*_{jj})^{1/2}\delta_{ij} \tag{6}$$

where ϵ^*_{ii} and ϵ^*_{jj} are the characteristic mer−mer interaction energies for components i and j and δ_{ij} is another empirical binary parameter. The number of sites occupied by a molecule of the mixture, r_{mix}, can be calculated from the following mixing rule:

$$\frac{1}{r_{mix}} = \sum_{i=1}^{nc}\frac{\phi_i}{r_i} \tag{7}$$

where r_i is the number of sites that a molecule of species i occupies in the lattice. The interphase partitioning of monomer and carbon dioxide has been evaluated by equating the corresponding chemical potential in each phase, μ_i, estimated through the following relationship:[9]

$$\mu_i = RT\left[\ln\phi_i + \left(1 - \frac{r_i}{r_{mix}}\right)\right] + r_i\left\{-\tilde{\rho}\left[\frac{2}{v^*_{mix}}\left(\sum_{j=1}^{nc}\phi_j v^*_{ij}\epsilon^*_{ij} - \epsilon^*_{mix}\sum_{j=1}^{nc}\phi_j v^*_{ij}\right) + \epsilon^*_{mix}\right] + RT\tilde{v}\left[(1-\tilde{\rho})\ln(1-\tilde{\rho}) + \frac{\tilde{\rho}}{r_i}\ln\tilde{\rho}\right] + p\tilde{v}\left(2\sum_{j=1}^{nc}\phi_j v^*_{ij} - v^*_{mix}\right)\right\} \tag{8}$$

where $\tilde{\rho} = 1/\tilde{v}$ is the reduced density. The Sanchez−Lacombe EOS is applied to each phase and, combined with the constraint of constant reactor volume ($V_{reactor} = V_1 + V_2^{tot}$), provides the volumes of the two phases, V_j, and the overall pressure, p. Note that in agreement with assumption 5 the volume of the polymer phase, $V_2 = V_2^{tot} - V_2^{cryst}$, used in all calculations is actually only the amorphous part of the total polymer volume. The crystal fraction was assumed to be constant during the reaction and set to 65% as obtained experimentally by DSC.

Population Balance Equations (PBE) for Active and Terminated Polymer Chains. The equations used in this work have been modified with respect to

the previous ones[2] in order to include the chain transfer to polymer reaction:

$$\frac{dR_{x,j}}{dt} = k_{pj}[M_j][R_{x-1,j}]V_j(1-\delta(x-1)) + 2f_j k_{dj}[I_j]V_j\delta(x-1) - (k_{pj}[M_j] + (k_{tdj}+k_{tcj})\sum_{y=1}^{\infty}[R_{y,j}])[R_{x,j}]V_j - K_{x,j}A_p([R_{x,j}] - [R^*_{x,j}]) - k_{fpj}[R_{x,j}]V_j\sum_{y=1}^{\infty}y[P_{y,j}] + k_{fpj}x[P_{x,j}]V_j\sum_{y=1}^{\infty}[R_{y,j}] \quad (9)$$

$$\frac{dP_{x,j}}{dt} = \frac{1}{2}k_{tcj}\sum_{y=1}^{x-1}[R_{y,j}][R_{x-y,j}]V_j + k_{tdj}[R_{x,j}]V_j\sum_{y=1}^{\infty}[R_{y,j}] - K_{x,j}A_p([P_{x,j}] - [P^*_{x,j}]) + k_{fpj}[R_{x,j}]V_j\sum_{y=1}^{\infty}y[P_{y,j}] - k_{fpj}x[P_{x,j}]V_j\sum_{y=1}^{\infty}[R_{y,j}] \quad \text{for } j = 1, 2 \text{ and } x = [1, \infty] \quad (10)$$

where $\delta(x - x_0)$ indicates the Kronecker delta function, defined as equal to 1 for $x = x_0$ and 0 otherwise.

It is worth noting that, in the frame of this model, the only required information about the polymer phase morphology is the overall interphase surface area, which, assuming equal spherical polymer particles, is given by $A_p = 4\pi r_p^2 N_p$. In the following we use the final value of the polymer particle specific surface area, a_p^f, as an adjustable parameter and estimate the number of particles under the assumption of spherical geometry as follows:

$$N_p = \frac{X^f m^0_{VDF}\rho_{PVDF}{}^2 a_p^{f\,3}}{36\pi} \quad (11)$$

where X^f is the final conversion (at which a_p^f has been obtained), m^0_{VDF} the total initial monomer mass, and ρ_{PVDF} the density of the polymer. During the reaction N_p is assumed constant in time, and since the dispersed phase volume V_2 obviously increases, we can back compute the increase in time of r_p and of the specific surface area as reported by eq 1, and from this the value of the total particle surface area which is the only morphological parameter in the model:

$$A_p = \frac{a_p^{f3}}{a_p{}^2}X^f m^0_{VDF} \quad (12)$$

Note that as a consequence of assumption 4 above, very small values of A_p would lead to an accumulation of polymer chains in the supercritical phase such as to promote homogeneous nucleation that is however not accounted for in this model.

More details about the numerical solution of the resulting system of mixed algebraic−differential equations can be found in our previous work.[2]

4. Parameter Evaluation

The reliable evaluation of the large number of model parameters is always a critical issue when developing a detailed kinetic model. In this work, whenever possible, these have been estimated from independent experimental data to minimize the fitting of the available experimental polymerization runs and to enhance model reliability. All the parameter numerical values and the corresponding sources are listed in Table 2 while their derivation is discussed in the following.

4.1. Kinetic parameters: Continuous Phase. The following Arrhenius-type expressions have been used in order to account for temperature and pressure dependencies of the kinetic rate constants:

$$k(T,p_0) = A\exp\left(-\frac{E}{RT}\right) \quad (13)$$

$$k(T,p) = k(T,p_0)\exp\left(-\frac{\Delta V^{\#}}{RT}(p-p_0)\right) \quad (14)$$

where A is a preexponential factor, E the activation energy, $\Delta V^{\#}$ the activation volume, and p_0 the reference pressure, usually equal to the pressure at which the values of k are available.

Propagation. No value could be found for the VDF propagation reaction in the literature. However, for the aqueous microemulsion copolymerization of VDF/HFP (hexafluoropropylene), Apostolo et al.[10] reported an overall propagation rate constant, $\overline{k_p}$ of 2100 L mol^{-1} s^{-1} at 80 °C and 2.2 MPa. Even though evaluated under different conditions, it is quite reasonable to use the same value in supercritical CO_2 since it has been reported that the solvent effect on the propagation rate coefficient of different vinyl monomers (styrene and methyl methacrylate) is practically nonobservable.[11] Moreover, Beuermann et al.[12] measured a k_p difference between polymerization in bulk and in supercritical CO_2 less than a factor 2. The selected value was defined as the average of the propagation rate constants, k_{pA} and k_{pB}, of the two radical species corresponding to monomers A (VDF) and B (HFP):

$$\overline{k_p} = \frac{k_{pA}[A] + k_{pB}[B]}{[A] + [B]} \quad (15)$$

Applying the pseudo-kinetic approximation, k_{pA} and k_{pB} are given as follows:

$$k_{pA} = k_{pAA}\mathscr{P}_A + \frac{k_{pBB}}{r_B}\mathscr{P}_B \quad (16)$$

$$k_{pB} = k_{pBB}\mathscr{P}_B + \frac{k_{pAA}}{r_A}\mathscr{P}_A \quad (17)$$

where $\mathscr{P}_i$ is the probability of having a radical chain with end group of type i, k_{pAA} and k_{pBB} are the homopolymerization constants, and r_A and r_B are the reactivity ratios. For the system VDF/HFP the latter are equal to 2.9 and 0.12, respectively.[13] Note that this set of values is different from that we used in a previous paper,[10] and it has been selected because evaluated more recently. Moreover, it is well-known that HFP does not homopolymerize which means that $k_{pBB} \ll 1$. Thus, the overall propagation rate constant for this system can be approximated by the following expression:

$$\overline{k_p} \approx k_{pAA}\mathscr{P}_A\left(x_A + \frac{1-x_A}{r_A}\right) \quad (18)$$

Table 2. Model Parameter Values and Sources

parameter	units	reference
	Kinetic Parameters: Continuous Phase	
$f_{1,0} = 0.6$		reference 20
$A_{d1} = 6.3 \times 10^{16}$	s^{-1}	reference 20
$E_{d1} = 132$	kJ mol^{-1}	reference 20
$\Delta V^{\#}_{d1} = 0$	cm^3 mol^{-1}	reference 20
$p_{0,d1} = 27.6$	MPa	reference 20
$A_{p1} = 6.4 \times 10^5$	L mol^{-1} s^{-1}	reference 10, this work
$E_{p1} = 15$	kJ mol^{-1}	references 14,15, typical value
$\Delta V^{\#}_{p1} = -25$	cm^3 mol^{-1}	references 14−16, typical value
$p_{0,p1} = 2.2$	MPa	reference 10
$A_{p/\sqrt{t},1} = 6.5 \times 10^9$	$L^{1/2}$ $mol^{-1/2}$ $s^{-1/2}$	reference 18, this work
$E_{p/\sqrt{t},1} = 70$	kJ mol^{-1}	reference 18, this work
$\Delta V^{\#}_{t1} = 15$	cm^3 mol^{-1}	references 14−16, 19, typical value
$p_{0,p/\sqrt{t},1} = 23.4$	MPa	reference 18
$k_{fp1}/k_{p1} = 1.0 \times 10^{-6}$		fitted
	Kinetic Parameters: Dispersed Phase	
$f_{2,0} = 0.6$		reference 20
$A_{d2} = 6.3 \times 10^{16}$	s^{-1}	reference 20
$E_{d2} = 132$	kJ mol^{-1}	reference 20
$\Delta V^{\#}_{d2} = 0$	cm^3 mol^{-1}	reference 20
$p_{0,d2} = 27.6$	MPa	reference 20
$A_{p2} = 6.4 \times 10^5$	L mol^{-1} s^{-1}	reference 10, this work
$E_{p2} = 15$	kJ mol^{-1}	references 14,15, typical value
$\Delta V^{\#}_{p2} = -25$	cm^3 mol^{-1}	references 14−16, typical value
$p_{0,p2} = 2.2$	MPa	reference 10
$A_{p/\sqrt{t},2} = 6.5 \times 10^9$	$L^{1/2}$ $mol^{-1/2}$ $s^{-1/2}$	reference 18, this work
$E_{p/\sqrt{t},2} = 70$	kJ mol^{-1}	reference 18, this work
$\Delta V^{\#}_{t2} = 15$	cm^3 mol^{-1}	references 14−16,19, typical value
$p_{0,p/\sqrt{t},2} = 23.4$	MPa	reference 18
$k_{fp2}/k_{p2} = 1.0 \times 10^{-6}$		fitted
	Free Volume Parameters	
$D_0 = 7.66 \times 10^{-4}$	cm^2 s^{-1}	by fitting data from reference 36
$E = 8.21 \times 10^2$	J mol^{-1}	by fitting data from reference 36
$K_{1,VDF}/\gamma = 1.04 \times 10^{-3}$	cm^3 g^{-1} K^{-1}	by fitting data from reference 36
$K_{1,PVDF}/\gamma = 6.22 \times 10^{-5}$	cm^3 g^{-1} K^{-1}	by fitting data from reference 35
$K_{2,VDF} - T_{g,VDF} = -0.6$	K	by fitting data from reference 36
$K_{2,PVDF} - T_{g,PVDF} = 330$	K	by fitting data from reference 35
$V^*_{VDF} = 0.690$	cm^3 g^{-1}	references 33, 34
$V^*_{CO_2} = 0.589$	cm^3 g^{-1}	references 47, 48
$V^*_{PVDF} = 0.565$	cm^3 g^{-1}	references 33, 34
$V^{ref}_{FH,CO_2} = 0.231$	cm^3 g^{-1}	references 47, 48
$\alpha_{CO_2} = 8.76 \times 10^{-4}$	K^{-1}	references 47, 48
$\xi_{VDF/PVDF} = 0.484$		references 33, 37
$\xi_{VDF/CO_2} = 0.284$		references 33, 37
	Thermodynamic Parameters	
VDF		
$\epsilon^* = 2{,}632$	J mol^{-1}	by fitting data from reference 35
$v^* = 7.76$	cm^3 mol^{-1}	by fitting data from reference 35
$r = 6.03$		by fitting data from reference 35
CO_2		
$\epsilon^* = 2{,}536$	J mol^{-1}	reference 49
$v^* = 4.41$	cm^3 mol^{-1}	reference 49
$r = 6.60$		reference 49
PVDF		
$\epsilon^* = 6{,}652$	J mol^{-1}	reference 39
$v^* = 20.16$	cm^3 mol^{-1}	reference 39
$\rho^* = 1.920$	g cm^{-3}	reference 39
binary interactions		
$\delta_{VDF/CO_2} = 0.925$		by fitting data from reference 40
$\delta_{VDF/PVDF} = 0.820$		fitted
$\delta_{CO2/PVDF} = 0.925$		by fitting data from reference 40
$\eta_{VDF/CO_2} = 0.838$		by fitting data from reference 40
$\eta_{VDF/PVDF} = 1.000$		assumed
$\eta_{CO2/PVDF} = 0.840$		by fitting data from reference 40
initiator partitioning		
$K_{DEPDC} = 1.0$		this work
oligomer partitioning		
$\alpha_1 = -0.04$		by fitting data from reference 45
$\alpha_2 = -0.2$		by fitting data from reference 45
$m_{11} = 4.04 \times 10^{-1}$		reference 45
$m_{27} = 9.25 \times 10^{-2}$		reference 45
particle surface area		
$a^f_p = 0.27$	m^2 g^{-1}	fitted

where x_A is the molar fraction of monomer A in the reaction mixture. Under the conditions reported in ref 10, a value of 3870 L mol^{-1} s^{-1} is estimated for the VDF homopolymerization constant, k_{pAA}. Using an activation energy $E_p = 15$ kJ mol^{-1} (typical for vinyl halogens[14,15]) and an activation volume $\Delta V^{\#}_p = -25$ cm^3 mol^{-1}

(typical for vinyl monomers[14−16]), an initial value of 2850 L mol^{-1} s^{-1} is obtained at the operating conditions of the experimental run 1 in Table 1.

Chain Transfer to Polymer. The presence of this reaction has been indicated by Maccone et al.,[17] who found branching in the case of terpolymers of VDF, HFP, and tetrafluoroethylene (TFE). This result is relevant to indicate the existence of branching in VDF polymerization because this terpolymer is composed primarily of VDF (72%) and branching on HFP and TFE is unlikely, since these contain only C−F bonds. Moreover, Saraf et al.[4] found a solid mass of polymer at increased monomer concentrations that was not soluble in any solvent, which indicates that branching or even gelation can occur in the polymerization system under examination here. In the same work a value of 2.6 × 10^{-3} for the ratio between the chain transfer to polymer rate constant, k_{fp1}, and the propagation rate constant, k_{p1}, has been obtained by fitting experimental polydispersity index (PDI) values. This value is expected to be quite overestimated due to the fact that this fitting was done using a model describing the polymerization in one phase only, while the presence of two polymerization loci certainly contributes to increase the PDI. Since the chain transfer to polymer reaction affects only the broadness of the MWD, the value of this specific ratio has been determined by fitting the experimental MWD data obtained in this work. As discussed later, a much smaller value has been obtained, i.e., 1 × 10^{-6}.

Bimolecular Termination. Charpentier et al.[18] proposed an Arrhenius-type relationship for the ratio between the propagation rate constant and the square root of the termination rate constant, $k_{p1}/\sqrt{k_{t1}}$, at constant density. Accordingly, they evaluated the corresponding "effective" activation energy $E_{p/\sqrt{t,1}} = 78$ kJ mol^{-1}. However, to properly account also for the pressure dependence, the relationship (14) has been used, and using the above-reported activation volume for the propagation reaction and 15 cm^3 mol^{-1} for the termination reaction (typical value for vinyl monomers[14−16,19]), a corrected value of the "effective" activation energy $E_{p/\sqrt{t,1}} = 70$ kJ mol^{-1} has been estimated. Since there is no evidence in the literature for a significant contribution of termination by disproportionation,[4] termination by combination is assumed to be the unique bimolecular termination mechanism.

Initiator Decomposition. The first-order reaction rate constant for the decomposition of DEPDC in $scCO_2$ has been estimated using the values of activation energy, E_{d1}, and preexponential factor, A_{d1}, reported by Charpentier et al.[20] and equal to 132 kJ mol^{-1} and 6.3 × 10^{16} s^{-1}, respectively. Note that neither a significant pressure effect nor a noticeable dependence on the solvent type has been observed by the same authors. About the initiator efficiency, values around 0.6 were estimated for temperatures between 65 and 85 °C in the same work, where no clear temperature dependency was observed.

4.2. Kinetic Parameters: Dispersed Phase. Since the polymer concentration within the particles remains quite large all along the reaction (weight fraction around 0.8 in the amorphous part), diffusion limitations on the kinetic processes have to be accounted for. In particular, these have been evaluated using a Fickian description of the reactant diffusion with diffusion coefficients estimated through the free volume theory. The adopted relationships are summarized below, while more detailed treatments are available in our previous contribution[1] as well as in the literature:[21−24]

$$f_2 = \left[1 - \frac{D_{VDF,0}}{D_{VDF}}\left(1 - \frac{1}{f_{2,0}}\right)\right]^{-1} \tag{19}$$

$$k_{p2} = \left(\frac{1}{k_{p2,0}} + \frac{1}{4\pi\sigma_{VDF}D_{VDF}N_A}\right)^{-1} \tag{20}$$

$$k_{t2}(x,y) = \left(\frac{1}{k_{t2,0}} + \frac{1}{4\pi r_{xy}(D_{x,com} + D_{y,com} + k_{p2}[M_2]a^2/3)N_A}\right)^{-1} \tag{21}$$

where D_{VDF} is the monomer diffusion coefficient evaluated in the frame of the free volume theory of Vrentas and Duda,[25−27] σ_{VDF} the Lennard-Jones diameter of the monomer, r_{xy} the separation at which the termination between chains of length x and y is instantaneous, a the root-mean-square end-to-end distance divided by the square root of the number of monomer units in the chain, and $D_{x,com}$ the center-of-mass diffusion coefficient for a chain of length x evaluated from the following universal scaling law:[28]

$$D_{x,com} = D_{VDF}x^{-(0.664+2.02\omega_{PVDF})} \tag{22}$$

being ω_{PVDF} the polymer weight fraction. It is worth noting that the actual values of $k_{t2}(x,y)$ used in this work are the simple arithmetic averages of the two values obtained from eq 21 using minimum and maximum values of r_{xy} ($r_{xy} = \sigma_{VDF}$, rigid chain limit, and $r_{xy} = 2aj_c^{1/2}$, flexible chain limit, j_c being the entanglement spacing).[29]

The values of the kinetic rate constants for the dispersed phase at zero conversion are set equal to the corresponding values for the continuous phase.

Note that using eq 19 the initiator efficiency in the dispersed phase is estimated to be about 3 times smaller than in the continuous phase as reported above.[20] This means that, contrary to the case of PMMA,[1,2] the radical production is expected to be significant in both phases.

4.3. Mass Transfer Coefficient. The mass transfer coefficient required in the population balance equations (9) and (10) is evaluated according to the two-film theory,[30,31] yielding the following expressions for the overall mass transfer coefficients referred to the two phases:

$$K_{x,1} = \left(\frac{1}{k_{x,1}} + \frac{m_x}{k_{x,2}}\right)^{-1} \tag{23}$$

$$K_{x,2} = \left(\frac{1}{m_x k_{x,1}} + \frac{1}{k_{x,2}}\right)^{-1} \tag{24}$$

The local transport coefficients are given by

$$k_{x,j} = \frac{D_{x,j}}{\delta_j} \tag{25}$$

where $D_{x,1}$ is evaluated using the correlation by Lusis and Ratcliff,[32] $D_{x,2}$ is obtained from eq 22, and δ_j is a characteristic length, in this work estimated as the particle radius. Figure 1 shows the overall mass transfer coefficient referred to the continuous phase, $K_{x,1}$, as a function of the chain length. It can be seen that for short

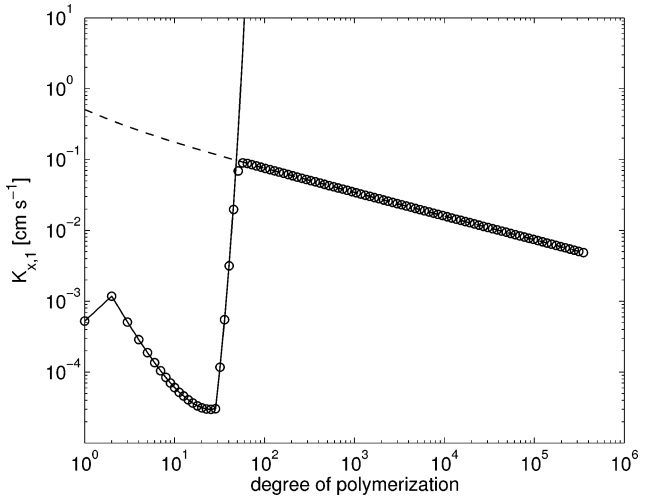

Figure 1. Overall mass transfer coefficient referred to the continuous phase, $K_{x,1}$ (○), and local contributions of the continuous phase, $k_{x,1}$ (dashed line), and the dispersed phase, $k_{x,2}/m_x$ (solid line), as a function of chain length (cf. eq 23).

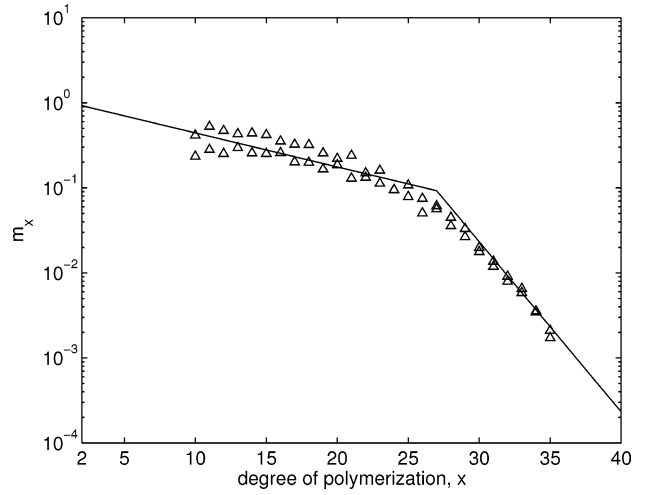

Figure 2. Chain partition coefficient as a function of chain length; experimental data from ref 45 (△) and fitted curve using eq 26 (line).

chains this coefficient is dominated by the transport within the polymer film whereas at increasing chain length the local transport in the continuous phase gets more and more important and is completely dominating for chains containing more than about 60 monomer units. Note that the behavior of the overall mass transfer coefficient for long chains is the result of the rapid decrease of the chain partition coefficient, m_x, at increasing x (cf. Figure 2).

4.4. Free Volume Parameters. The evaluation of the diffusion coefficient through the free volume theory requires the knowledge of several physical quantities, as described in detail in ref 1. For brevity, we do not repeat here the entire treatment, but we simply discuss how the values of the various parameters involved, which are summarized in Table 2, have been estimated. For pure CO_2, the same values used in our previous work have been considered here. The pure component parameters for VDF and PVDF have been either estimated from or fitted to their pure component properties.[33] In particular, the specific hole free volume, V_i^*, has been estimated from the molar volume at 0 K, which in turn was evaluated by the group contribution method of Sugden.[34] The free volume parameters of the polymer, $K_{1,PVDF}/\gamma$ and $K_{2,PVDF} - T_{g,PVDF}$, were obtained by fitting the experimental temperature dependence of viscosity provided by Solvay-Solexis[35] through the modified Williams−Landel−Ferry equation (cf. ref 33). The corresponding parameters for the monomer were obtained in a similar way but adopting Doolittle's expression for the viscosity−temperature relationship (cf. ref 33) and the experimental data taken from ref 36. About the ratio of the critical molar volume of the jumping units, ξ, the expression proposed by Ju et al. was considered.[37] Finally, the preexponential factor, D_0, and the critical energy required to overcome the attractive forces, E, have been estimated by combining the Dullien equation[38] for the self-diffusion coefficient of pure solvents with the Vrentas−Duda free volume equation in the limit of pure solvents, as proposed in ref 33.

4.5. Thermodynamic Parameters. As mentioned above, the Sanchez−Lacombe EOS has been used to describe the PVT behavior and the phase partitioning of the multicomponent system under examination. This equation requires three pure component parameters for each component as well as two binary interaction parameters for each component pair.

Pure Component Parameters. Briscoe et al.[39] reported Sanchez−Lacombe pure component parameters of PVDF at 42 and 80 °C. Since the experimental data considered in the present work were obtained at 50 °C (cf. Table 1), the values at the lower temperature have been used. For CO_2 the same set of values of pure component parameters as in our previous contribution[2] was considered here. About VDF, since no data are available in the literature, the corresponding parameter values were evaluated by fitting a set of PVT experimental data obtained by Solvay-Solexis.[35]

Binary Interaction Parameters. The sorption data at 42 and 60 °C reported in ref 40 have been used in order to evaluate the binary interaction parameters of PVDF/CO_2. About the interaction between VDF and CO_2, experimental data of density as a function of pressure at 42 and 60 °C for the binary mixture with $x_{VDF} = 0.103$ have been used to estimate the corresponding binary parameters.[40] Concerning VDF/PVDF interactions, the only information available in the literature is a qualitative indication of very limited monomer solubility in its polymer.[3,40] Therefore, the parameter $\delta_{VDF/PVDF}$ has been estimated by direct fitting of the experimental reaction data while $\eta_{VDF/PVDF}$ has been set equal to one, thus neglecting entropic interactions.

Initiator Interphase Partitioning. No data of interphase partitioning for the adopted initiator (DEPDC) have been found in the literature. However, reported partitioning data of dyes and a number of other organic species between supercritical carbon dioxide and different polymers indicate equipartitioning (i.e., $K_i = 1$) when the system pressure is large enough, usually above 10−15 MPa.[41,42] Since a similar behavior can reasonably be expected in the case of DEPDC, a species exhibiting special affinity to the polymer, the value $K_{DEPDC} = 1$ has been used in this work.

Polymer Interphase Partitioning. An empirical expression for the chain length dependent partition coefficient in $scCO_2$, similar to that reported for polystyrene (PS)[43] and PMMA,[44] has been used:

$$\begin{cases} \log m_x = \log m_{11} + \alpha_1(x - 11) & 2 \le x \le 27 \\ \log m_x = \log m_{27} + \alpha_2(x - 27) & x > 27 \end{cases} \quad (26)$$

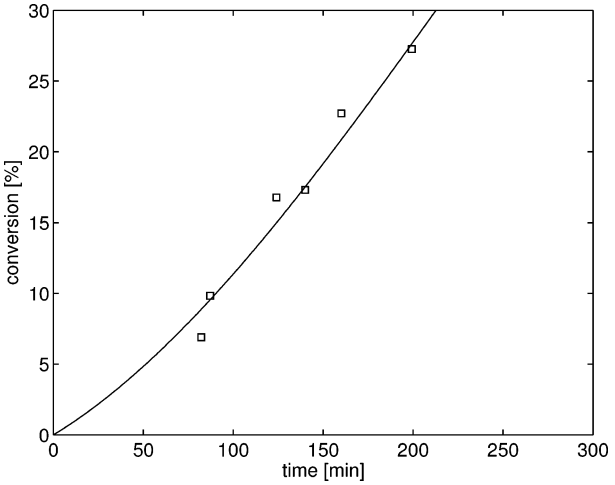

Figure 3. Conversion as a function of reaction time calculated by the model (line) and measured experimentally (□) for the base case (run 1 in Table 1).

where the values of m_{11}, m_{27}, α_1, and α_2 have been obtained by fitting the data reported in ref 45 (cf. Figure 2). Since these data have been measured at conditions not too far from the ones reported in Table 1, the values of the parameters in eq 26 have been kept constant in all simulations, thus neglecting any temperature and pressure effect. This last assumption has been verified by Bonavoglia et al.[45] for the system PS/CO_2. Of course, the partition coefficient of the species of length 1 (i.e., monomer and monomeric radical) has been computed with the Sanchez−Lacombe EOS.

4.6. Adjustable Quantities. Even though most of the model parameters have been estimated from independent sources, three quantities were considered as adjustable parameters: the VDF/PVDF binary interaction parameter, $\delta_{VDF/PVDF}$, the chain transfer to polymer rate constant, k_{fpj}, and the final specific interphase surface area, a_p^f. Since the role of each parameter is different (the first and the last ones have significant impact on the whole system behavior, while the second one affects only the broadness of the MWD), it was possible to get reliable estimates of them by fitting a single specific experiment (base case), while using all the remaining ones to check the model predictive capabilities.

5. Model Validation

To check the reliability of the model developed in this work, its results are now compared to the experimental data. The model−experiment comparison has been carried out in terms of conversion vs time and MWD vs conversion. In particular, the effects of changing initial monomer concentration on one side and density (i.e., pressure) on the other have been analyzed. Note that the calculated MWDs have been obtained by accounting for the polymer produced in both phases, $P_x = \sum_{j=1}^{2} P_{x,j}$ as computed by the population balance equations (10), and thus the plotted functions, $x^2P_x/(\sum_{x=1}^{\infty} xP_x)$ are proportional to the experimental GPC results.

5.1. Base Case. As mentioned above, the experimental data corresponding to the base case (run 1 in Table 1) were used to evaluate the three adjustable parameters of the model. The parameter fitting was done in order to get good agreement between model and experimental results in terms of conversion (Figure 3) and MWD (Figure 4) as a function of time. The obtained

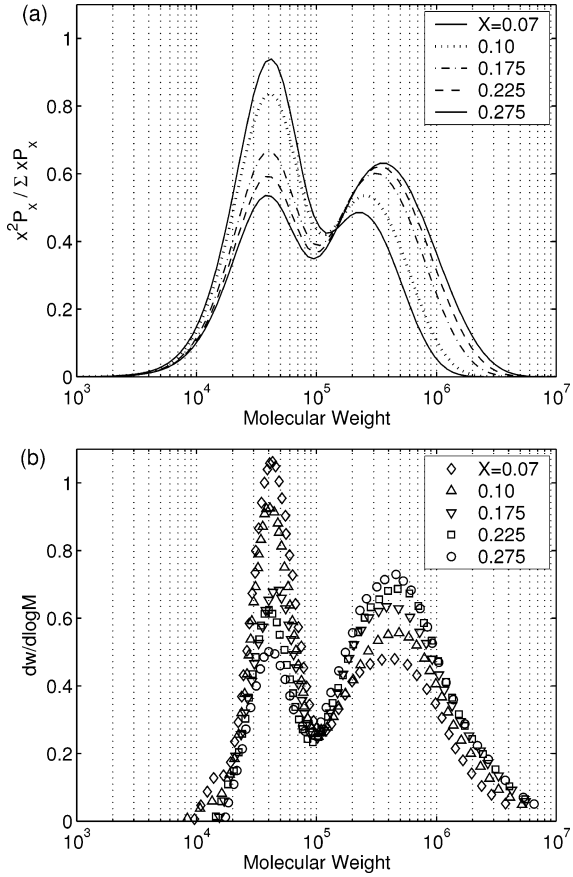

Figure 4. MWD at various conversions calculated by the model (a) and measured experimentally (b) for the base case (run 1 in Table 1).

values for the adjustable quantities ($\delta_{VDF/PVDF}$, k_{fpj}/k_{pj}, a_p^f) are given in Table 2.

The conversion curve in Figure 3 reveals an acceleration of the polymerization rate at increasing conversion which indicates some kind of gel effect. In Figure 4, it is seen that the MWD exhibits two modes: one in the low molecular weight region, corresponding to chains produced in the continuous phase, and the other one at higher molecular weights originated by chains formed in the polymer phase. The relative importance of these two fractions changes during the reaction, the shorter chains being predominant at low conversion. Looking at the shape of the two modes, it can be seen that the one at higher molecular weights is significantly broader than the other. Moreover, as the reaction proceeds, the higher molecular weight chains increase in average length while the shorter remain substantially constant. All these experimental observations are well reproduced by the model, thus enabling us to propose the following reaction mechanism.

The polymerization reaction proceeds in two loci: the continuous phase and the polymer particles. At low conversion, the first locus is dominant and low molecular weight chains are predominantly produced. Since no gel effect is operative in this phase, no acceleration is observed in the first part of the conversion vs time curve, and the first MWD mode is quite narrow, being the corresponding polydispersity about 1.5. On the other hand, as the reaction proceeds, the amount of polymer particles increases, leading to the fast increase of the relative importance of the second mode of the MWD, which becomes dominant after the first hour. Since the

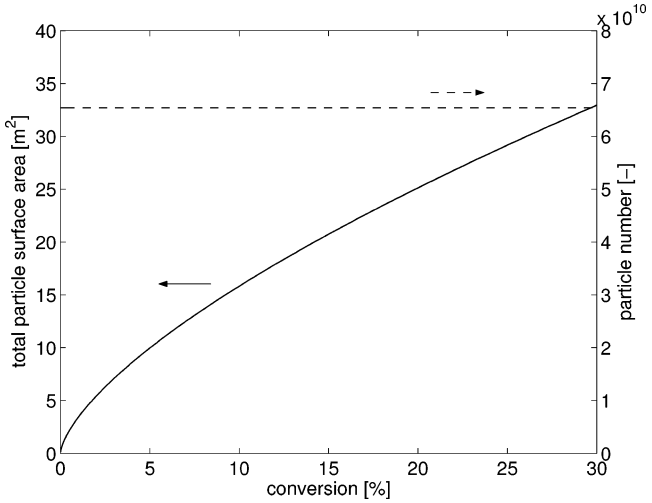

Figure 5. Total particle surface area (solid) and particle number (dashed) as a function of conversion for the base case (run 1 in Table 1).

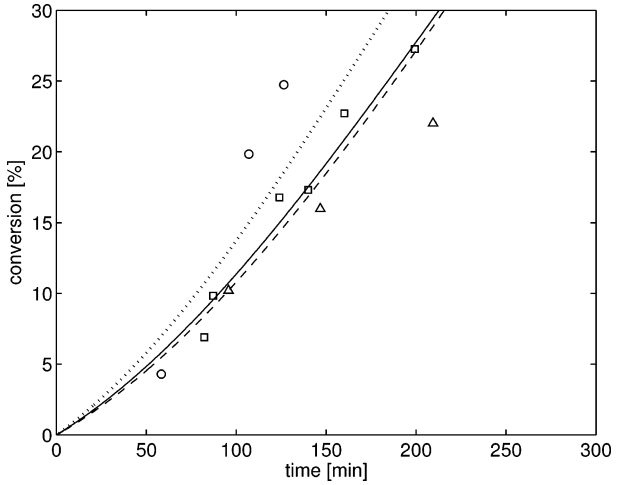

Figure 6. Conversion as a function of reaction time predicted by the model (lines) and measured experimentally: runs 4 (dashed, △), 1 (solid, □), and 5 (dotted, ○) in Table 1.

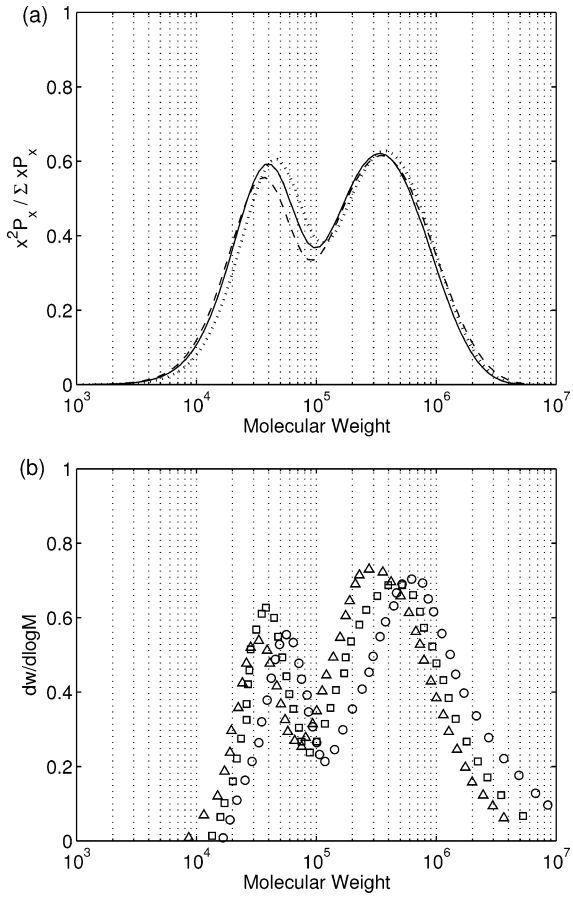

Figure 7. MWD at 25% conversion predicted by the model (a) and measured experimentally (b): runs 4 (dashed, △), 1 (solid, □), and 5 (dotted, ○) in Table 1.

termination rate in the polymer particles is significantly reduced by the gel effect, the MWD of the second mode exhibits larger values than the first one, and its average value increases with conversion. In addition, the conversion vs time curve undergoes the acceleration process typical of the gel effect. Finally, since the high molecular weight chains exhibit larger probability to undergo chain transfer to polymer reaction, this mode of the MWD is significantly broader than the first one.

It is worth repeating that the obtained value for the ratio between the polymer chain transfer reaction rate constant and k_p reported in Table 2 is about 3 orders of magnitude smaller than the one reported by Saraf et al.[4] As anticipated, this is due to the fact that Saraf et al. used an homogeneous model to fit the experimental polydispersity values. These are very high because the experimental MWD exhibits bimodality, which is however not predicted by the homogeneous model. Since in our model bimodality is properly accounted for by the presence of two reaction loci, the extent of branching to polymer needed to reproduce the experimental polydispersities is much smaller.

About the particle morphology, a constant number of spherical particles was assumed to be present from the beginning of the reaction so as to reproduce a certain value of the final specific interphase surface area (assumption 4). Typical evolutions of the total particle surface area and of the particle number computed under this assumption are shown in Figure 5.

5.2. Effect of Density. About the density effect on reaction rate and MWD, at least for the range of density values investigated in this work, no significant trend is found, neither experimentally nor in the model predictions (cf. Figures 6 and 7). This observation is in agreement with the findings of Hsiao et al.[46] for dispersion polymerization of MMA in $scCO_2$. Although as a whole, taking also the experimental errors into consideration, this result is satisfactory, a more detailed analysis is possible. A closer inspection of Figures 6 and 7 reveals some density effects, i.e., a slight increase of the polymerization rate and a small shift of the two modes of the MWD toward higher molecular weights at increasing density. This can be the result of the effect of density on various parameters in conflict with each other. In fact, changing the system density affects the kinetic rate constants as well as the interphase partitioning of both monomer and CO_2. Larger densities usually correspond to larger propagation rate constant and smaller termination rate constant (cf. activation volumes in Table 2), which in turn leads to increased polymerization rates and higher molecular weights. About the effect on partitioning, higher densities increase the sorption of CO_2 in the dispersed phase which results in the dilution of the latter and, therefore, in the reduction of all diffusion limitations on the chemical reactions. As a consequence, larger termination and initiation rates are expected, thus resulting in shorter

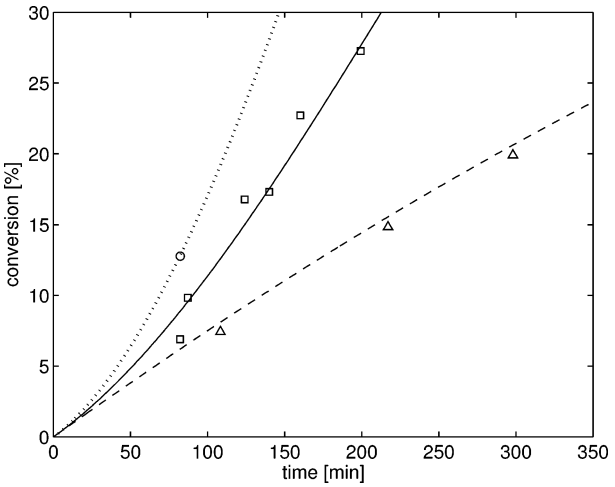

Figure 8. Conversion as a function of reaction time predicted by the model (lines) and measured experimentally: runs 2 (dashed, △), 1 (solid, □), and 3 (dotted, ○) in Table 1.

chain lengths. Moreover, Saraf et al.[3] reported a decrease of the monomer partitioning coefficient between polymer and continuous phase at increasing densities, from which reduced polymerization rate and, once more, lower molecular weights would be expected. Thus summarizing, changes of the density of the polymerization system affect several factors leading to changes of the polymerization rate and the molecular weights of the produced chains in opposite directions. Looking at the model predictions, it is seen that the experimentally observed increase of the polymerization rate is reproduced, even though in a less distinct way (cf. Figure 6). On the other hand, higher molecular weights with increasing density are only predicted for the chains produced in the continuous phase (cf. Figure 7a) whereas the experimental MWD exhibits a shift of both modes as shown in Figure 7b. This small discrepancy between model and experiments could also be due to the assumption of constant value of the specific polymer particle surface area at the end of the reaction in all experimental runs.

5.3. Effect of Monomer Concentration. Figure 8 shows conversion as a function of reaction time at three different monomer concentrations. A nice agreement between model predictions and experimental data is found. It is interesting to note that, in the case of the lowest monomer concentration, the reaction rate does not exhibit any acceleration, thus indicating that the polymerization is predominantly occurring in the continuous phase. As the monomer concentration increases, the main reaction locus shifts toward the dispersed phase, thus leading to a significant increase of the polymerization rate due to the presence of gel effect in the dispersed phase.

A further confirmation to this interpretation is given by the results shown in Figure 9 where the calculated final MWDs are compared to the experimental ones. At increasing monomer concentration a second mode grows in the high molecular weight region, as a result of the increased importance of the reaction in the dispersed phase. Note that this second mode becomes dominant at the same time when acceleration appears in the reaction rate, which is in agreement with the predicted switch of the main reaction locus from the continuous to the dispersed phase.

Since the same value of the final specific surface area, a_p^f, has been assumed in all simulations, the number of

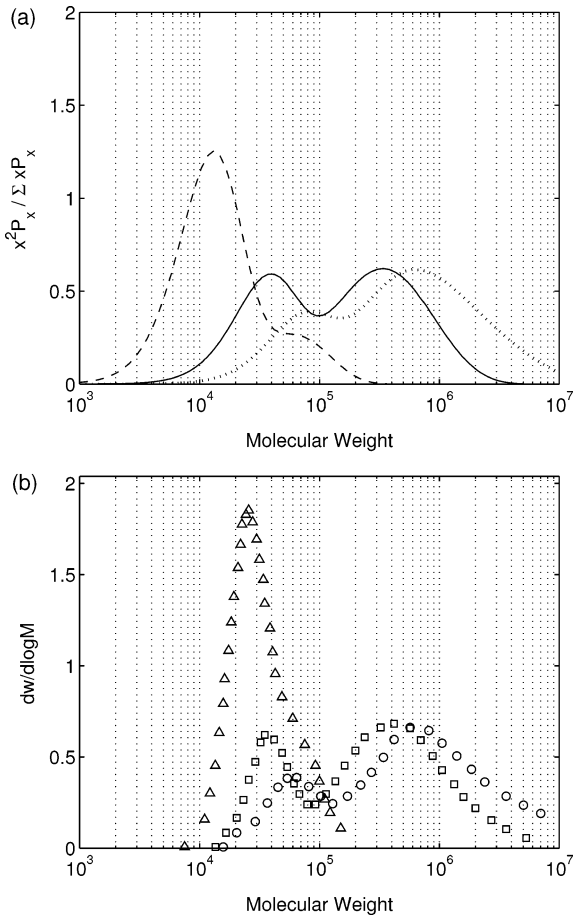

Figure 9. MWD at 25% conversion predicted by the model (a) and measured experimentally (b): runs 2 (dashed, △), 1 (solid, □), and 3 (dotted, ○) in Table 1.

particles is different at different monomer concentrations and found to have the following values: $N_p = 2.1 \times 10^{10}$ at $[M]_0 = 1.0$ mol L^{-1}, 6.5×10^{10} at 3.1 mol L^{-1}, and 13.1×10^{10} at 6.2 mol L^{-1}.

6. Discussion

To determine the main reaction locus of heterogeneous polymerization in $scCO_2$, we need to compare the characteristic times of interphase mass transport and termination. This is conveniently done through the parameter Ω defined for each phase, j as a function of chain length, x as follows:[1,2]

$$\Omega_j(x) = \frac{K_{x,j}A_p}{\sum_{y=1}^{\infty} k_{tj}(x,y)[R_{y,j}]V_j} \tag{27}$$

where $K_{x,j}$ is the overall mass transfer coefficient with respect to phase j and A_p the total interphase surface area. Ω values above one indicate that chain transport is faster than termination, which means that the active chains can leave the original phase before they terminate, thus continuing their growth and eventually terminate in the other phase. On the other hand, Ω values below one mean that the active chains are terminated in the phase where they are formed, thus leading to a segregated system. In the case of heterogeneous polymerization in $scCO_2$ only the transport of the active chains from the continuous phase to the

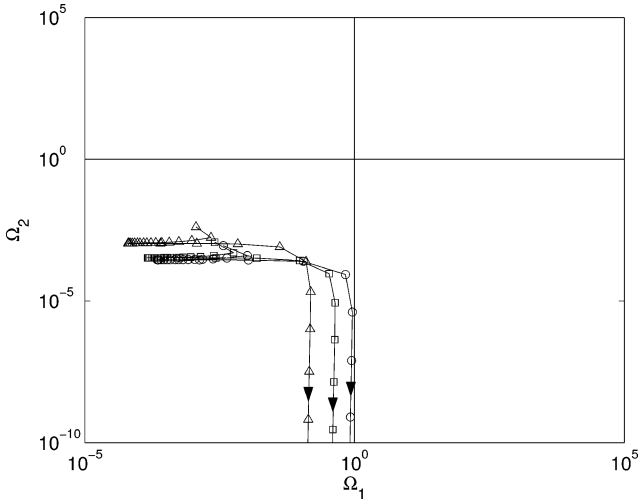

Figure 10. Ω plot calculated at 25% conversion under the operating conditions of runs 2 (△), 1 (□), and 3 (○) in Table 1; arrows indicate increasing degree of polymerization.

particles needs to be discussed, while the opposite transfer is always negligible, i.e., $\Omega_2 \ll 1$.[1] Moreover, the behavior of $\Omega_1(x)$ can be understood by looking at the behavior of $K_{x,1}$ shown in Figure 1.

In the case of the system under examination here, the bimodal MWDs indicate that two main reaction loci are operative. This means that part of the radicals generated in the continuous phase terminate in the same phase before being able to reach the dispersed phase, as requested by their equilibrium partitioning. Therefore, Ω_1 values smaller than one are expected for the active chains. In Figure 10 the Ω values calculated by the model for the reactions carried out at three different monomer concentrations (i.e., runs 1−3 in Table 1) and at 25% conversion are shown at increasing degree of polymerization. As expected, it is found that both Ω_1 and Ω_2 are always clearly smaller than one, except for Ω_1 at the largest degree of polymerization where values very close to one are obtained. This indicates that we are not far from the situation where the active chains originated in the continuous phase diffuse in the polymer particles, thus giving rise to a system where only one polymerization locus is active. In Figure 10 the larger Ω_1 values obtained at the larger monomer concentrations indicate that the contribution of the continuous phase as a polymerization locus is smaller, as it is confirmed by the smaller area of the first mode of the MWDs shown in Figure 9.

To better illustrate this point, we have performed a few simulations where the particle specific surface area has been artificially increased in order to favor the transport of the radicals in the polymer particles. As shown in Figure 11, the first mode of the MWD tends to disappear as soon as the Ω_1 values for the larger radicals exceed unity as shown in the inset of the same figure.

On the other hand, if we do not allow the radicals to diffuse from the continuous to the dispersed phase, i.e., we adopt the assumption of complete segregation of the active chains, then the model predicts the reaction to take place predominantly in the continuous phase, leading to a MWD largely different from the experimental one, as shown in Figure 12. It is seen that most of the polymer is in this case produced in the continuous phase (i.e., low molecular weight). This is because the monomer is much more soluble in the supercritical

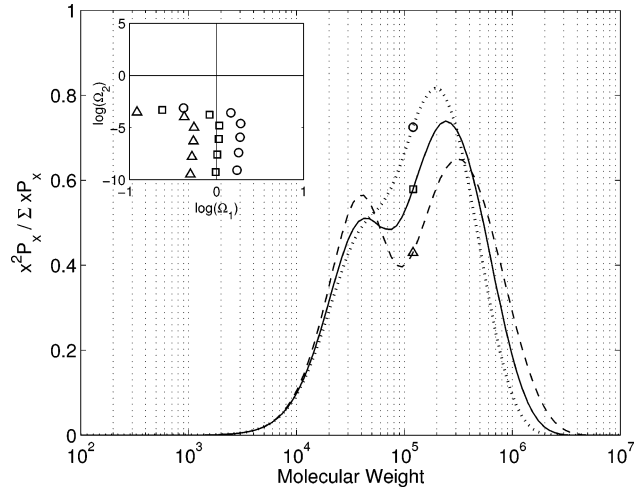

Figure 11. MWD predicted by the model under the operating conditions of run 1 in Table 1 at increased values of the final specific polymer particle surface area: $a_p^f = 0.30$ m^2 g^{-1} (dashed, △), $a_p^f = 0.40$ m^2 g^{-1} (solid, □), $a_p^f = 0.50$ m^2 g^{-1} (dotted, ○); inset shows the corresponding Ω plots.

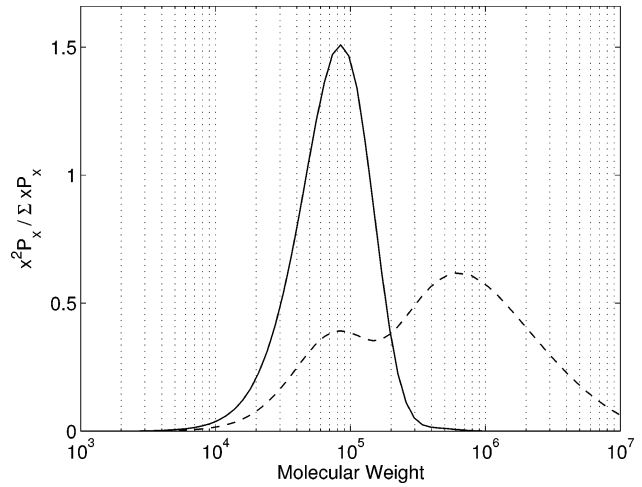

Figure 12. MWD predicted by the model under the operating conditions of run 3 in Table 1 (dashed, same curve as the dotted one in Figure 9a) and MWD under the same conditions without interphase transport of active chains (solid).

phase than in the polymer phase. This observation underlines the importance of describing in detail the transport of the radicals to the polymer particles. If such transport would be infinitely fast, we would obtain again a monomodal MWD like in the case of a segregated system, but this time centered around large molecular weights (i.e., produced in the polymer phase) as shown in Figure 11. The bimodality of the MWD observed experimentally can only be reproduced by correctly modeling the competition between diffusion and termination for the radicals moving from the continuous to the dispersed phase. Note that in the simulations above the dead polymer chains have been assumed not to be segregated, but rather to diffuse immediately to the polymer phase, so as to avoid an unrealistic accumulation in the supercritical phase.

The role of chain transfer to polymer is investigated in Figure 13 where the MWD predicted by the model (dashed line) is compared with the one that one would obtain in the absence of chain transfer to polymer (solid line). As mentioned above, this reaction broadens mainly the high molecular weight mode since the longer the chains, the larger the impact of this branching reaction.

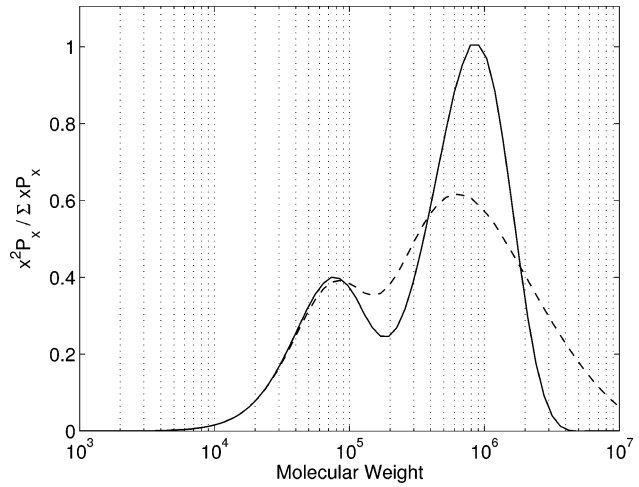

Figure 13. MWD computed by the model under the operating conditions of run 3 in Table 1 (dashed, same curve as the dotted one in Figure 9a) and MWD computed under the same conditions without chain transfer to polymer (solid).

It also appears that by further increasing this reaction rate one could probably induce a new mode in the MWD, but this would clearly occur at much larger values than those observed experimentally.

7. Conclusions

A model describing heterogeneous polymerization in $scCO_2$ has been applied to simulate the precipitation polymerization of VDF. After a careful evaluation of most of the model parameters based on independent literature information, the remaining three were evaluated by fitting one set of experimental data at given operating conditions and then kept constant for all the other conditions investigated experimentally. Very nice agreement between model predictions and experimental observations was found when changing the initial monomer concentration. The same comparison was satisfactory when varying the density of the system, although a very minor effect was found on both polymerization rate and MWD.

Moreover, the issue of the dominant reaction locus was analyzed. Since radicals are generated in both dispersed and continuous phase, we have potentially two polymerization loci. Given that low molecular weight species are at interphase equilibrium, the first one, i.e., the polymer particles, is always active, while the second one can be active or not depending on whether the active radicals generated in the continuous phase are transported or not to the dispersed phase before terminating. This situation, which is well described by the dimensionless Ω parameter,[1] depends on the specific conditions occurring during the process and cannot be predicted a priori. This implies that, to correctly describe the relative amount of polymer produced in each reaction locus, a detailed model accounting for the kinetics of the transport of the active chains from the continuous to the dispersed phase is needed. An important conclusion is that limiting models assuming interphase equilibrium partitioning or segregation (cf. ref 1) are not appropriate in this case, and they could result in significant mechanistic misunderstandings.

Acknowledgment. The financial support of BBW (Swiss Federal Office for Education and Science, Contract 02-0131, EC-Contract G1RD-CT-2002-00676, ECOPOL) and ETH (ETHZ—internal research project "Dispersion Polymerization in Supercritical Carbon Dioxide") is gratefully acknowledged.

Notation

a = root mean square end-to-end distance per square root of monomer units, cm
a_p^f = final specific particle surface area, $m^2\ g^{-1}$
A_p = total particle surface area, m^2
A_{dj} = preexponential factor of initiator decomposition in phase j, s^{-1}
A_{pj} = preexponential factor of propagation in phase j, L $mol^{-1}\ s^{-1}$
$A_{p/\sqrt{t},j}$ = preexponential factor of the ratio $k_{pj}/\sqrt{k_{tj}}$ in phase j, $L^{1/2}\ mol^{-1/2}\ s^{-1/2}$
$[A]$ = concentration of monomer A, mol L^{-1}
$[B]$ = concentration of monomer B, mol L^{-1}
D_0 = preexponential factor of diffusion coefficient (free volume theory), $cm^2\ s^{-1}$
D_i = self-diffusion coefficient of component i, $cm^2\ s^{-1}$
$D_{i,0}$ = self-diffusion coefficient of component i at zero conversion, $cm^2\ s^{-1}$
$D_{x,com}$ = center-of-mass diffusion coefficient of a chain of length x, $cm^2\ s^{-1}$
E = critical energy to overcome attractive forces (free volume theory), J mol^{-1}
E_{dj} = activation energy of initiator decomposition in phase j, kJ mol^{-1}
E_{pj} = activation energy of propogation in phase j, kJ mol^{-1}
$E_{p/\sqrt{t},j}$ = activation energy of the ratio $k_{pj}/\sqrt{k_{tj}}$ in phase j, kJ mol^{-1}
f_j = initiator efficiency in phase j
$f_{j,0}$ = initiator efficiency in phase j at zero conversion
I_j = amount of initiator in phase j, mol
$[I_j]$ = initiator concentration in phase j, mol L^{-1}
$I_j^\bullet$ = amount of activated initiator in phase j, mol
l_c = entanglement spacing
k_{dj} = initiator decomposition rate constant in phase j, $1\ s^{-1}$
k_{fpj} = chain transfer to polymer rate constant in phase j, L $mol^{-1}\ s^{-1}$
k_{Ij} = initiation rate constant in phase j, L $mol^{-1}\ s^{-1}$
$\bar{k}_p$ = overall pseudo-homopolymerization propagation rate constant, L $mol^{-1}\ s^{-1}$
k_{pi} = pseudo-homopolymerization propagation rate constant of monomer i, L $mol^{-1}\ s^{-1}$
k_{pii} = homopolymerization propagation rate constant of monomer i, L $mol^{-1}\ s^{-1}$
k_{pj} = propagation rate constant in phase j, L $mol^{-1}\ s^{-1}$
$k_{pj,0}$ = propagation rate constant in phase j at zero conversion, L $mol^{-1}\ s^{-1}$
k_{tj} = termination rate constant in phase j, L $mol^{-1}\ s^{-1}$
$k_{tj,0}$ = termination rate constant in phase j at zero conversion, L $mol^{-1}\ s^{-1}$
k_{tcj} = termination by combination rate constant in phase j, L $mol^{-1}\ s^{-1}$
k_{tdj} = termination by disproportionation rate constant in phase j, L $mol^{-1}\ s^{-1}$
$k_{x,j}$ = local mass transfer coefficient in phase j, cf. eq 25, cm s^{-1}
$K_{1,i}$ = free volume parameter of component i, $cm^3\ g^{-1}\ K^{-1}$
$K_{2,i}$ = free volume parameter of component i, K
K_i = partition coefficient of component i
$K_{x,j}$ = overall mass transfer coefficient of a chain of length x referred to phase j, cf. eqs 23 and 24, cm s^{-1}
m_i^0 = total initial mass of component i, g
m_x = partition coefficient of a chain of length x, cf. eq 26
M_j = amount of monomer in phase j, mol
$[M_j]$ = monomer concentration in phase j, mol L^{-1}
nc = number of components
N_A = Avogadro number, mol^{-1}
N_p = particle number
p = pressure, MPa

$p_{0,dj}$ = reference pressure at which k_{dj} has been obtained, MPa
$p_{0,pj}$ = reference pressure at which k_{pj} has been obtained, MPa
$p_{0,p}/\sqrt{}_{t,j}$ = reference pressure at which $k_{pj}/\sqrt{k_{tj}}$ has been obtained, MPa
P_x = total amount of terminated polymer chains of length x in both phases, mol
$P_{x,j}$ = amount of terminated polymer chains of length x in phase j, mol
$[P_{x,j}]$ = concentration of terminated polymer chains of length x in phase j, mol L^{-1}
$[P^*_{x,j}]$ = hypothetical concentration of terminated polymer chains of length x in phase j in equilibrium with the corresponding bulk concentration in the other phase, mol L^{-1}
r_{mix} = number of lattice sites occupied by a molecule in the mixture, cf. eq 7
r_i = number of lattice sites occupied by component i
r_i = reactivity ratio
r_p = particle radius, cm
r_{xy} = separation at which termination between chains of length x and y is instantaneous, cm
R = universal gas constant, J mol^{-1} K^{-1}
$R_{x,j}$ = amount of radical chains of length x in phase j, mol
$[R_{x,j}]$ = concentration of radical chains of length x in phase j, mol L^{-1}
$[R^*_{x,j}]$ = hypothetical concentration of radical chains of length x in phase j in equilibrium with the corresponding bulk concentration in the other phase, mol L^{-1}
t = time, s
T = temperature, K
$T_{g,i}$ = glass transition temperature of component i, K
V_1 = volume of the continuous phase, L
V_2 = volume of the amorphous part of the dispersed phase, L
V_2^{cryst} = volume of the crystalline part of the dispersed phase, L
V_2^{tot} = total volume of the dispersed phase, L
$V_{FH,i}$ = specific hole free volume of component i, cm^3 g^{-1}
V_i^* = specific critical hole free-volume of component i, cm^3 g^{-1}
$V_{reactor}$ = reactor volume, L
x, y = chain length
x_i = mole fraction of species i
X = conversion
X^f = final conversion

Greek Letters

α_1, α_2 = chain partitioning parameter, cf. eq 26
α_i = coefficient of thermal expansion of component i, K^{-1}
γ = overlap factor (free volume theory)
δ_j = characteristic length of diffusion in phase j, cf. eq 25, cm
δ_{ij} = binary interaction parameter, cf. eq 6
$\delta(x - x_0)$ = Kronecker delta function
$\Delta V_{dj}^{\#}$ = activation volume of initiator decomposition in phase j, cm^3 mol^{-1}
$\Delta V_{pj}^{\#}$ = activation volume of propagation in phase j, cm^3 mol^{-1}
$\Delta V_{tj}^{\#}$ = activation volume of termination in phase j, cm^3 mol^{-1}
ϵ^*_{mix} = characteristic interaction energy of the mixture, cf. eq 5, J mol^{-1}
ϵ^*_{ii}, ϵ^*_i= characteristic interaction energy of component i, J mol^{-1}
ϵ^*_{ij}= characteristic interaction energy between component i and j, J mol^{-1}
η_{ij} = binary interaction parameter, cf. eq 3
μ_i = chemical potential of component i, cf. eq 8, J mol^{-1}
ξ_{ij} = ratio between molar volumes of jumping units of i and j
$\mathscr{P}_i$ = probability of having a radical chain with end group of type i
$\tilde{\rho}$ = reduced density
ρ_i = density of component i, g cm^{-3}
ρ_i^* = characteristic density of component i, g cm^{-3}
σ_i = Lennard-Jones diameter of component i, cm
$\tilde{v}$ = reduced molar volume
v^*_{mix} = characteristic molar volume of the mixture, cf. eq 2, cm^3 mol^{-1}
v^*_{ii}, v^*_i= characteristic volume of component i, cm^3 mol^{-1}
v^*_{ij} = characteristic volume of components i and j, cm^3 mol^{-1}
ϕ_i = site fraction of component i, cf. eq 4
ω_i = weight fraction of component i
$\Omega_j(x)$ = ratio between characteristic times of termination and interphase mass transport of a chain of length x in phase j, cf. eq 27

References and Notes

(1) Mueller, P. A.; Storti, G.; Morbidelli, M. *Chem. Eng. Sci.* **2005**, *60*, 377−397.
(2) Mueller, P. A.; Storti, G.; Morbidelli, M. *Chem. Eng. Sci.* **2005**, *60*, 1911−1925.
(3) Saraf, M. K.; Wojcinski, L. M., II; Kennedy, K. A.; Gerard, S.; Charpentier, P. A.; DeSimone, J. M.; Roberts, G. W. *Macromol. Symp.* **2002**, *182*, 119−129.
(4) Saraf, M. K.; Gerard, S.; Wojcinski, L. M.; Charpentier, P. A.; DeSimone, J. M.; Roberts, G. W. *Macromolecules* **2002**, *35*, 7976−7985.
(5) Fehrenbacher, U.; Muth, O.; Hirth, T.; Ballauff, M. *Macromol. Chem. Phys.* **2000**, *13*, 1532−1539.
(6) Fehrenbacher, U.; Ballauff, M. *Macromolecules* **2002**, *35*, 3653−3661.
(7) Sanchez, I.; Lacombe, R. *J. Phys. Chem.* **1976**, *80*, 2352−2368.
(8) Sanchez, I.; Lacombe, R. *Macromolecules* **1978**, *11*, 1145−1156.
(9) McHugh, M. A.; Krukonis, V. J. *Supercritical Fluid Extraction*, 2nd ed.; Elsevier: Newton, 1994.
(10) Apostolo, M.; Arcella, V.; Storti, G.; Morbidelli, M. *Macromolecules* **2002**, *35*, 6154−6166.
(11) Morrison, B. R.; Piton, M. C.; Winnik, M. A.; Gilbert, R. G.; Napper, D. H. *Macromolecules* **1993**, *26*, 4368−4372.
(12) Beuermann, S.; Buback, M.; Schmaltz, C.; Kuchta, F. D. *Macromol. Chem. Phys.* **1998**, *199*, 1209−1216.
(13) Souzy, R.; Ameduri, B.; Boutevin, B. *Macromol. Chem. Phys.* **2004**, *205*, 476−485.
(14) Odian, G. *Principles of Polymerization*; McGraw-Hill: New York, 1970.
(15) Brandrup, J.; Immergut, E. H. *Polymer Handbook*, 4th ed.; John Wiley & Sons: New York, 1998.
(16) Ogo, Y.; Yokawa, M. *Macromol. Chem.* **1977**, *178*, 453−464.
(17) Maccone, P.; Apostolo, M.; Ajroldi, G. *Macromolecules* **2000**, *33*, 1656−1663.
(18) Charpentier, P. A.; DeSimone, J. M.; Roberts, G. W. *Ind. Eng. Chem. Res.* **2000**, *39*, 4588−4596.
(19) Ogo, Y.; Kyotani, T. *Macromol. Chem.* **1978**, *179*, 2407−2417.
(20) Charpentier, P. A.; DeSimone, J. M.; Roberts, G. W. *Chem. Eng. Sci.* **2000**, *55*, 5341−5349.
(21) Allen, P. E. M.; Patrick, C. R. *Kinetics and Mechanisms of Polymerization Reactions*; John Wiley & Sons: New York, 1974.
(22) North, A. M. *The Collision Theory of Chemical Reactions in Liquids*; John Wiley & Sons: London, 1964.
(23) Noyes, R. M. In *Progress in Reaction Kinetics*; Porter, G., Ed.; Pergamon Press: Oxford, 1961; Vol. 1, p 131.
(24) Litvinenko, G. I.; Kaminsky, V. A. *Prog. React. Kinet.* **1994**, *19*, 139−193.
(25) Vrentas, J. S.; Duda, J. L. *J. Polym. Sci., Polym. Phys. Ed.* **1977**, *15*, 403−416.
(26) Vrentas, J. S.; Duda, J. L. *J. Polym. Sci., Polym. Phys. Ed.* **1977**, *15*, 417−439.
(27) Vrentas, J. S.; Duda, J. L.; Ling, H.-C. *J. Polym. Sci., Polym. Phys. Ed.* **1984**, *22*, 459−469.
(28) Griffiths, M. C.; Strauch, J.; Monteiro, M. J.; Gilbert, R. G. *Macromolecules* **1998**, *31*, 7835−7844.
(29) Russell, G. T.; Napper, D. H.; Gilbert, R. G. *Macromolecules* **1988**, *21*, 2133−2140.
(30) Lewis, W. K.; Whitman, W. G. *Ind. Eng. Chem.* **1924**, *16*, 1215−1239.

(31) Treybal, R. E. *Mass Transfer Operations*; McGraw-Hill: New York, 1968.
(32) Lusis, M. A.; Ratcliff, G. A. *Can. J. Chem. Eng.* **1968**, *46*, 385−387.
(33) Hong, S.-U. *Ind. Eng. Chem. Res.* **1995**, *34*, 2536−2544.
(34) Haward, R. N. *J. Macromol. Sci., Rev. Macromol. Chem.* **1970**, *C4*, 191−242.
(35) Internal data, Solvay-Solexis, S.p.A, Bollate (Italy), 2003.
(36) Daubert, T. E.; Danner, R. P.; Sibul, H. M.; Stebbins, C. C. *Physical and Thermodynamic Properties of Pure Chemicals. Data Compilation.*; Taylor & Francis: Washington, 1989.
(37) Ju, S. T.; Duda, J. L.; Vrentas, J. S. *Ind. Eng. Chem. Prod. Res. Dev.* **1981**, *20*, 330−335.
(38) Dullien, F. A. L. *AIChE J.* **1972**, *18*, 62−70.
(39) Briscoe, B. J.; Lorge, O.; Wajs, A.; Dang, P. *J. Polym. Sci., Part B: Polym. Phys.* **1998**, *36*, 2435−2447.
(40) Kennedy, K. A. Characterization of Phase Equilibrium Associated with Heterogeneous Polymerizations in Supercritcal Carbon Dioxide. Ph.D. Thesis, North Carolina State University, 2003.
(41) Condo, P. D.; Sumpter, S. R.; Lee, M. L.; Johnston, K. P. *Ind. Eng. Chem. Res.* **1996**, *35*, 1115−1123.
(42) Kazarian, S. G.; Vincent, M. F.; West, B. L.; Eckert, C. A. *J. Supercrit. Fluids* **1998**, *13*, 107−112.
(43) Kumar, S. K.; Chhabria, S. P.; Reid, R. C.; Suter, U. W. *Macromolecules* **1987**, *20*, 2550−2557.
(44) Bonavoglia, B.; Verga, U.; Storti, G.; Morbidelli, M. Paper presented at AIChE Annual Meeting, San Francisco, CA, Nov 16−21, 2003. Session: 96-Polymerization and Polymer Processing with Supercritical Fluids II.
(45) Bonavoglia, B.; Storti, G.; Morbidelli, M. *Macromolecules*, published online June 4, 2005, http://dx.doi.org/10.1021/ma0505068.
(46) Hsiao, Y. L.; Maury, E. E.; DeSimone, J. M.; Mawson, S.; Johnston, K. P. *Macromolecules* **1995**, *28*, 8159−8166.
(47) Alsoy, S.; Duda, J. L. *AIChE J.* **1998**, *44*, 582−590.
(48) Gupta, R. R.; Lavery, K. A.; Francis, T. J.; Webster, J. R. P.; Smith, G. S.; Russell, T. P.; Watkins, J. J. *Macromolecules* **2003**, *36*, 346−352.
(49) Kiszka, M. B.; Meilchen, M. A.; McHugh, M. A. *J. Appl. Polym. Sci.* **1988**, *36*, 583−597.

MA0504522